DOI: 10.31534/engmod.2021.1.ri.01m
Original scientific paper
Received: 11.09.2020.

Evaluation the effect of particle sphericity on direct shear mechanical behavior of granular materials using discrete element method (DEM)

Muath S. Talafha[1], **Istvan Oldal**[2]

[1] *Department of Mechanics and Engineering Design, Szent István University, Gödöllö, H-2103, pest, HUNGARY*
e-mail: muath.talafha@gmail.com

[2] *Department of Mechanics and Engineering Design, Szent István University, Gödöllö, H-2103, pest, HUNGARY*
e-mail: oldal.istvan@gek.szie.hu

SUMMARY

Granular materials are an essential component of many fields, such as the medicine and agriculture industries, where their behavior is affected by the properties of constituent particles. The Discrete Element Method (DEM) is a potential technique used to describe the mechanical behavior of granular materials by making a mechanical model which describes the affected parameters, and one of these parameters is the shape of particles. It is an important characteristic that is represented by a sphericity index. In this study, the macro and micro-mechanical shear behaviors of granular materials are investigated using the Discrete Element Method (DEM). For this purpose, a three-dimensional (3D) program (EDEM) was developed on the basis of (DEM) and was used to model various particle shapes for a direct shear test. An assembly with a different particle center distance was prepared. The results showed a changing relationship between shear strength and the sphericity index, and micro-mechanical responses showed that particle shape affected the shape and the thickness of the shear zone.

KEY WORDS: *Discrete Element Method; granular materials; particle shape; direct shear test.*

1. INTRODUCTION

Granular materials are a major element of the pharmaceutical and agricultural industries. In general, the mechanical behavior of the granular material layer is influenced by the loading properties [1]; [2]; [3]; [4], distribution of particle size [5]; [6]; [7], fouling level [8]; [9]; [10]; [11], void ratio [4], confining pressure and normal stress [3] as well as the characteristics of individual particles, such as particle size [12]; [13]; [6] particle shape [14]; [9]; [15]; [16], and strength [17].

The angularity of the particles and their surface texture are the primary factors affecting the response of granular materials [18]. Ref. [19] showed that degradation of particles depends on particle form. Flaky or elongated particles are more likely to break than cubic ones. However, in experimental work, it is not easy to provide a clear way to visualize the evolution of particle angularity or its surface texture. Moreover, computer simulations are widely used in granular materials investigations due to the high cost of experiments and the heavy equipment limitations in performing large-scale studies.

Numerical models based on the discrete element method (DEM) have been developed in recent decades to investigate granular material behavior. Due to discrete complexity, DEM makes it possible to compare the results obtained by modifying the properties of the simulated materials especially [20], shape indexes. Ref. [21] performed a 2D simulation and concluded that the shear strength, dilation, and residual shear strength increased significantly as the particle angularity increased. Nevertheless, to represent the true nature of such particles remains a challenge in DEM simulations. In the DEM scheme [22] particle shape, such as disk or spherical, could only be modelled in 2D and 3D simulations. Although a simple algorithm is used to detect contacts and measure forces, the actual shape of the particle should be modelled since the rotation resistance of the disk or sphere is much lower than that of the actual particle shape. In disks or sphere particles, rotation is only caused by tangential contact forces and the moment does not contribute because normal forces are directed towards the core of the particles. Moreover, the point of interaction with actual particles varies from that of spherical. For this reason, several researchers have developed new methods that take into account the actual shape of the particles [23]; [24]; [25]; [26]; [27]. In railway studies, some of these techniques were used to model the shapes of ballast particles.

In order to approximate the actual shape of ballast particles, a ballast settlement was predicted under cyclic loading using DEM on polygon particles [28]. The critical size of the ballast was tested by simulating full-scale ballast layers, and it was observed that particles less than half the size of theoretical maximum are not suitable [29]. A similar approach was considered when modelling ballasts in other experiments [30]; [31]; [32]; [33].Ref. [34] used circular bonded particle clusters to model a 2D angular ballast particle projection. A similar approach was applied with 3D simulations for ballast modelling [35].

However, particles shaped like ellipsoids [23], particles shaped like polygons [24], an elliptical particle with oval-shaped boundary [25], particles with an axis symmetry [26], and particles with dense clusters overlapping [27] do not reflect effectively the actual types of such particles. Also, some of those methods required significant computational time. Therefore, [36] suggested a simple algorithm (now commonly used in DEM) for simulating the shape of particles. In this method, the overlapping elements of the sphere are connected rigidly, in which the advantage is that a particle structure of different angles can be modelled using the same interaction laws as a single sphere. This approach has been used to model the exact form of ballast in different studies. Ref. [37] simulated geogrid-reinforced ballasts to assess the ideal position of the geogrid. Furthermore, [38] simulated a direct shear box test and the shear strength decreased as the degree of fouling increased as a consequence of reduced particulate friction. They found that a high degree of fouling increases the dilation of the ballast samples, in particular when they are under low normal stress. Furthermore, [39] stated that good agreement exists between laboratory data and DEM simulations of geogrid-stabilized coal-fouled ballast. Finally, fouling on a ballast bed decreased the sleeper's lateral resistance, particularly when the fouling material was on the ballast layer shoulder, as in [40]. Although most numerical studies concentrated on modelling the actual type of particles in different

conditions or mechanical responses to the ballast layer, the effects of shape properties on mechanical results are rarely recorded in-depth and are difficult to consider in laboratory testing.

As a continuation of previous experimental research on the effect of particle breakage and the fouling of fine materials under various gradations relating to the shear strength of the granular layer, a 3D simulation of the direct shear cylinder test was conducted by means of DEM to establish the effect of shape properties on the shear strength parameters of the granular layer [41]. The numerical simulation was carried out by modelling the center of the various particles. Different levels of normal stress were used to determine the effects of shape properties on the behavior of the granular layer for particle shapes at different particle center distances (sphericity index). In addition, microscopic measurements were used to test the effects of a particle shape index on shear behavior and shear zone of the granular layer and the macroscopic response.

2. DEM SIMULATION

The Discrete Element Method (DEM) models for the mechanical behavior of granular materials have been developed by applying the equation of motion for every single particle of the material assembly [42]. The forces arising during particle-particle and particle–wall interactions are calculated during the simulation circle, where a cycle involving a repeated application of Newtonian laws of motion to generate the acceleration, velocity, and displacement values of each particle is used. The newly found displacement is then used to determine the contact forces and torques in that place because of the particle interactions in their new position. This cycle repeats multiple times to model the bulk material's mechanical behavior [43]. This approach is ideal for analysing the special behavior and motion of granular materials [44] or to examine the effect of vibration [43]. Ref. [44] has shown that their validated discrete element model is applicable to the determination of the velocity distribution in a mixed flow dryer and that the system optimizes the dryer geometry. Ref. [45] predicted that with the help of discrete models, exact pressure distribution in a silo can be determined and analysed, and, therefore, the design process of these types of equipment simplified. DEM can also be used to analyse flow patterns, segregations, discharge rate, and influence of flow correction inserts in the silos. It can be seen that the applicability of the discrete element method is very wide. When DEM is used, the equations of motion of single particles are solved by a simulation cycle. Newton's second law of motion and the general rotational dynamic equation are repeatedly used to explain the movement of single particles. Contact forces and moments are calculated based on the displacement of particles in every time step. The behavior of particles and interactions depend on the geometry and the micromechanical properties of particles and their contacts. For modelling the mechanical behavior of soil [43], EDEM discrete element software was applied as a discrete element software using the Hertz Mindlin No-Slip optimal contact model.

2.1 SHEAR BOX SIMULATION

The test was conducted in a cylinder, as shown in Figure 1, which has *225 mm* high and *35 mm* in radius. The lower cylinder height was *75 mm* and was free to move under the fixed upper cylinder, with a height of *150 mm*. The horizontal displacement of the test device was

represented by a distance of about *2.5 cm* (i.e. about *15%* shear strain), which is suitable for recording peak shear stress of the particle sample. The vertical loading system will apply and sustain a constant normal load on the sample. The horizontal loading system may also apply the shearing force to the sample at a constant rate of displacement in a direction parallel to that of movement in the lower cylinder.

Several particles of the same shape and the same sizes were produced for each assembly series. The particles which fill the shear cylinder were compacted by normal gravity forces for all samples. To enable an effective sample comparison, the simulated testing was carried out in three steps. The assemblies created during the first stage were very fast as the program produced particles that had contact with neighboring particles but retained kinetic energy at this moment. Therefore, it took a certain amount of time before the particles could calm down and attain zero kinetic energy. During the second step, the required vertical load was applied to the assembly and the use of an almost equal diameter particle of the shear testing system and the correctly calculated density enabled the application of adequate vertical load. The spherical shape of the vertical load allowed us to prevent load weight tilting, which is a common problem during DEM shear tests [46]. The direct shear test was carried out at the final step by shifting the lower cylinder of the shear apparatus horizontally, while the vertical stress was maintained constant during shear.

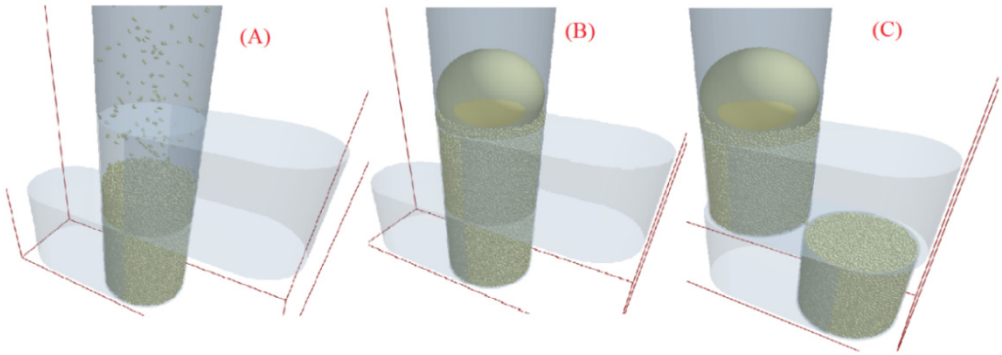

Fig. 1 *Simulation Shear box and the Stages of assembled generations particles with SPH of 88% under normal load of 16 N*
(A initially generated, B compacted and applied normal stress, C finally sheared)

2.2 MODEL PARAMETERS

A large-scale direct shear cylinder test is simulated, using a rigid wall with a freeloading dead weight sphere at the top of the upper cylinder. This would allow particles to move vertically during shearing. A total of 5 particles were selected in the simulations, and their sphericities were determined. The obtained values of the sphericities of the selected particles (SPH= *100%*, *98%*, *94%*, *88%*, *81%* of all the particles respectively) were considered during the DEM particle shape study.

For each repetition, the size of all particles in the DEM simulation was considered the same, to reduce gradation effects. Radius was 1mm for each particle, and there was a different distance between the double particle centers, at *0mm*, *0.5mm*, *1mm*, *1.5mm*, *1.9mm* respectively. Simulated direct shear tests were carried out under several vertical stresses.

The trial and error method was used to determine the DEM parameters, as shown in Table 1, in order for the simulation results to be acceptable.

Table 1 *Micromechanical parameters of the model*

Parameter	***Value***
Particles Poisson's ratio	*0.25*
Wall Poisson's ratio	*0.3*
Particles Shear modulus (Pa)	*1×10^8*
Wall Shear modulus (Pa)	*8×10^10*
Coefficient of restitution	*0.5*
Coefficient of rolling friction	*0.01*
Particle density (kg/m3)	*2500*
Coefficient of inter particle friction	*0.5*
Coefficient of plane wall-particle friction	*0.5*

2.3 PARTICLE SHAPE GENERATION

For the particle model, a variety of different sphericities were considered. The sphericity index (SPH) defined by [47] described sphericity as the ratio of the volume of the particles to that of the smallest circumscribing sphere. It was used to quantitatively analyse the shapes of the various particles.

For all practical shapes, the SPH value is between zero and one, with a value of one corresponding to a full sphere and zero correspondings to a very elongated particle. In Figure 2, the SPH values of all particles used in this study are presented.

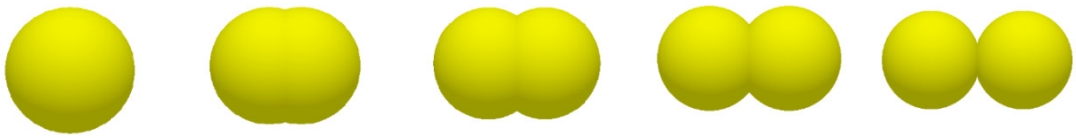

Fig. 2 *Various particle sphericity simulations*

(SPH = 100%, 98%, 94%, 88%, 81% for all the particles respectively)

3. SIMULATION RESULTS AND DISCUSSION

This section presents the macroscopic and microscopic findings explained in terms of the sphericity properties, the direct shear behavior of DEM numerical simulation for different particle samples. The results include volumetric strain, shear stress, the network of contact forces, variance in the contact number, and average particle rotation within the cylinders.

3.1 SHEAR STRESS

Upcoming figures present the variety of shear stress versus the horizontal strain for particle samples with a sphericity index under constant normal stresses. Measuring the arctangent of shearing stress ratio to normal stress ($\varphi = arctng\ (\tau.\sigma)$), the internal angle of friction was calculated. It was seen that the internal friction angle is inversely correlated with the particle sphericity. The effect of sphericity on internal friction is that the peak friction angle initially tends to reach its limit when the sphericity decreases with much lower values. This reduction in sphericity is considered relevant, and its effect is high. Similar findings were recorded for 2D elliptical particles. Refs. [23] and [48] have similar results for 3D ellipsoid multi-sphere assemblies.

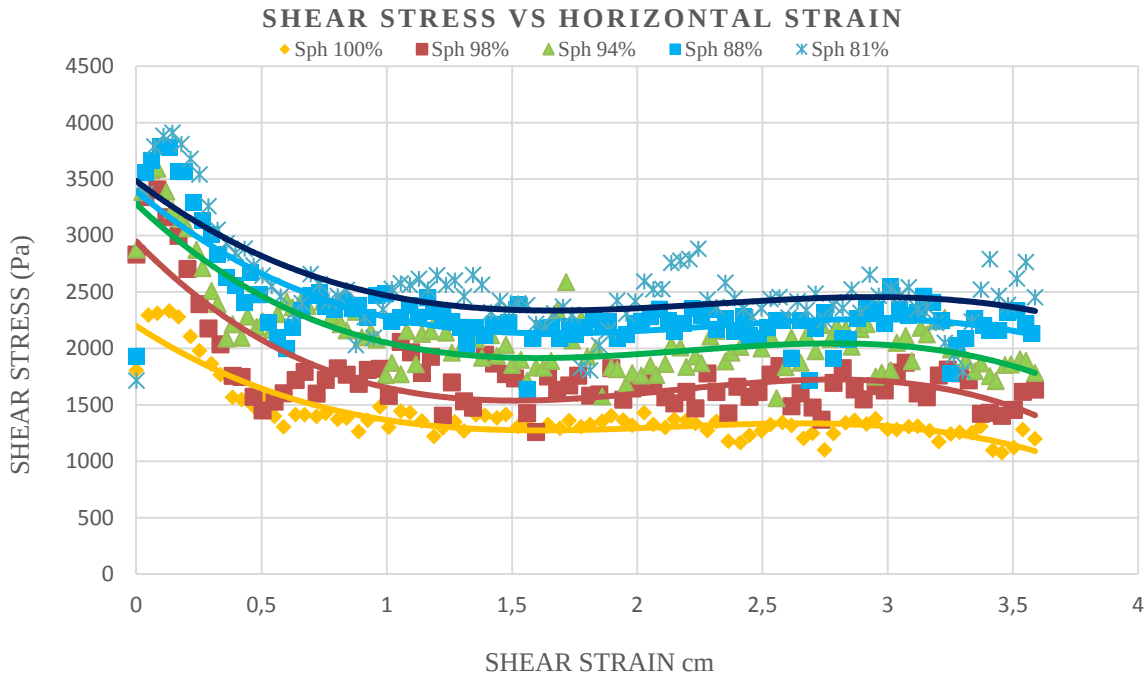

Fig. 3 *Shear stress–shear strain curves of samples with various sphericity at a normal stress of 4150 Pa*

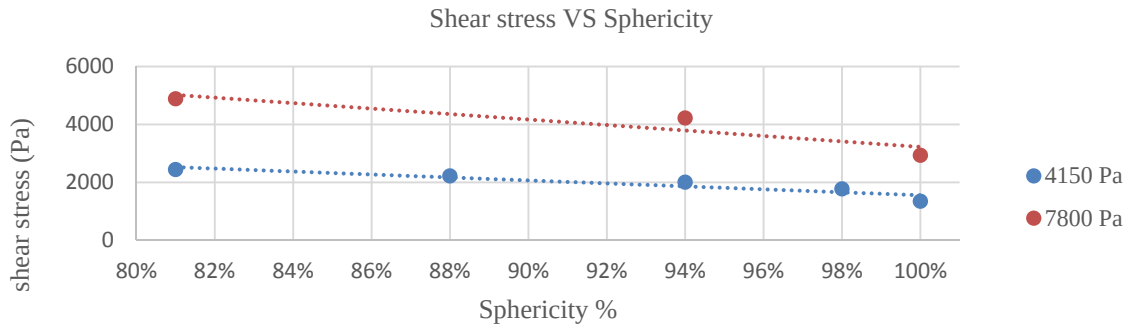

Fig. 4 *Shear stress with various sphericity at a normal stress of 4150 Pa and 7800 Pa*

The effect of sphericity on particle specimens is more apparent. This phenomenon illustrates the growing interlocking connections between particles under normal pressure, where the longer particles are more interlocked. For example, for normal stress of *4150 Pa*, the shear stress increased from *1300 Pa* to *2800 Pa* when the shape of the rounded particles changed to

the non-spherical particle (Sph=*81%*). However, the rate of increase in shear stress decreased for strongly spherical particles and vice versa.

There was a need to evaluate better the effects of the sphericity index on the shear behavior of particles at constant normal stress. Figure 3 shows the reflection of the sphericity index on the particles shear stress, where the lower sphericity index values caused an increase in the interlocking value between particles, leading to an increase of the shear stress. Secondly, Figure 4 shows that interlocking particles can be dilated due to a decrease in pressure on the particles, causing a decrease in shear strength. By decreasing the sphericity index, the particle experiences a greater amount of particle interlocking, which, in turn, causes a gradual increase in shear stress. In comparison, these particles are not able to move easily against each other due to high normal stress, which creates anisotropy. Less anisotropy in the sample contributes to a lower friction angle [49]. Thirdly, the shear strength of the particle samples increases with sphericity. For instance, shear stress increases by about *10%.* As the shape of particles changes from spherical to elongated, sphericity decreases from *100%* to *98%* for normal stress of *4150 Pa*.

3.2 VOLUMETRIC STRAIN

A comparison of the volumetric strain changes versus horizontal strain under different normal stresses is presented in Figure 5. It is seen that, as normal stress increases, the overall volumetric strain decreases, reflecting a lower dilation level under higher normal stress. Figure 6 shows that dilatancy in larger strains increases dramatically with an increase in sphericity, suggesting that dilatancy depends on the particle shape features and normal stress.

The dilation values for an assembly with less spherical particles (SPH=*81%*) is *44%* smaller than that of an assembly with SPH values of *100%*, at a normal stress of *4150 Pa*. Figure 7 shows that at higher normal stresses a lower level of dilation occurs in comparison to lower normal stresses.

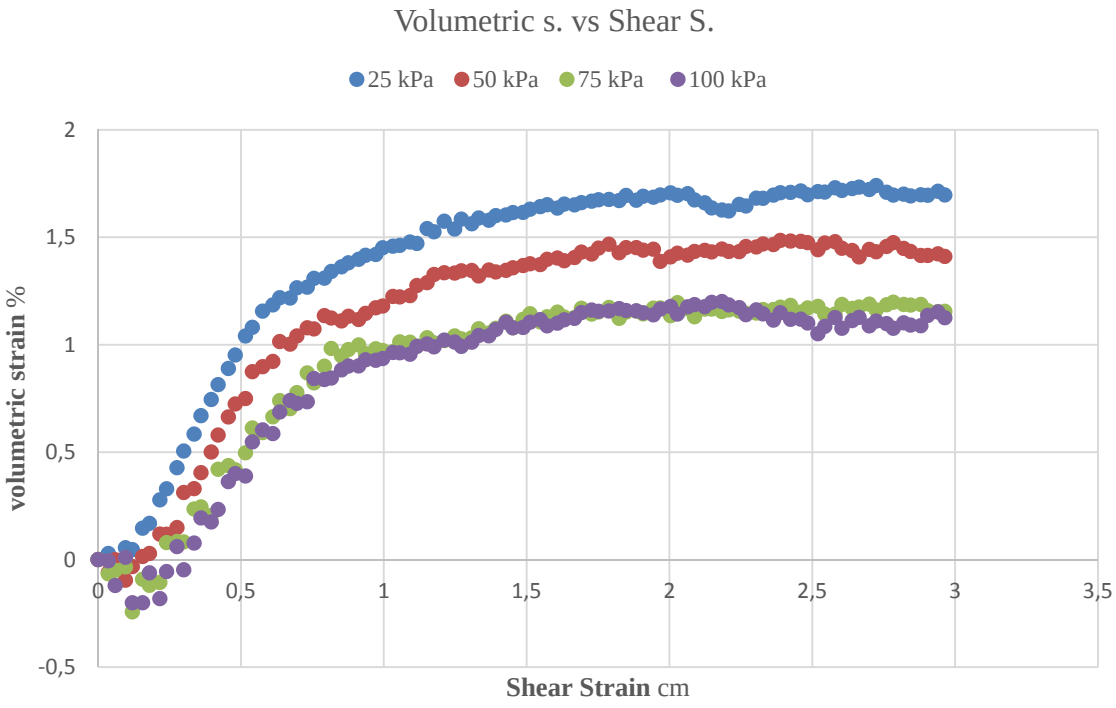

Fig. 5 *Variation of volumetric-shear strain for various normal stresses (1.9mm test)*

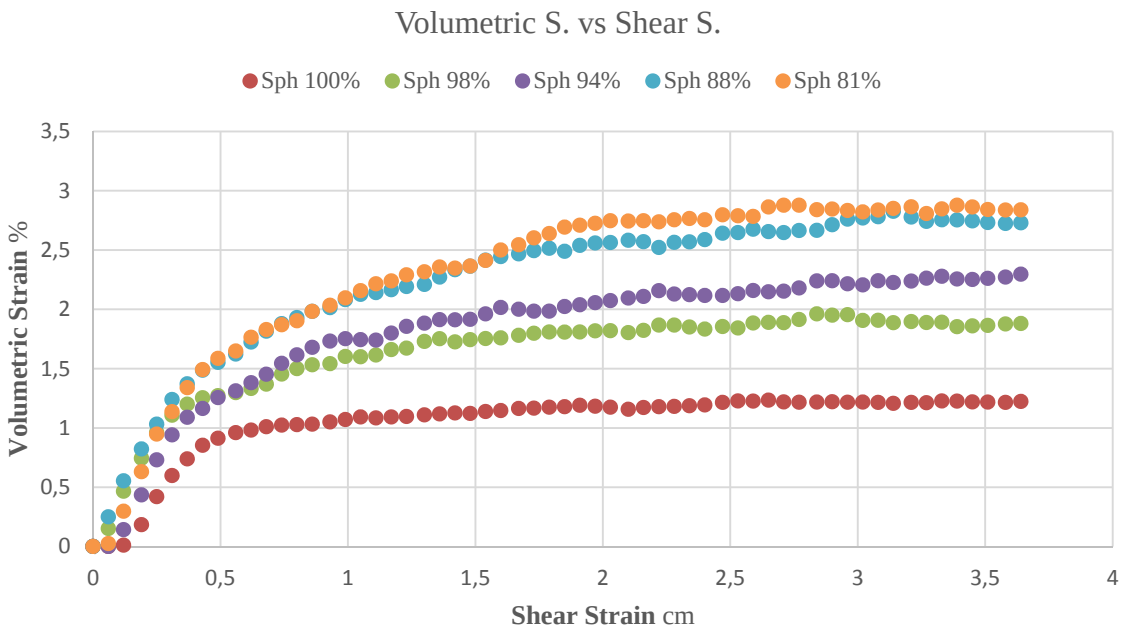

Fig. 6 *Variation of volumetric-shear strain for normal stress of 4150 Pa (sphericity index)*

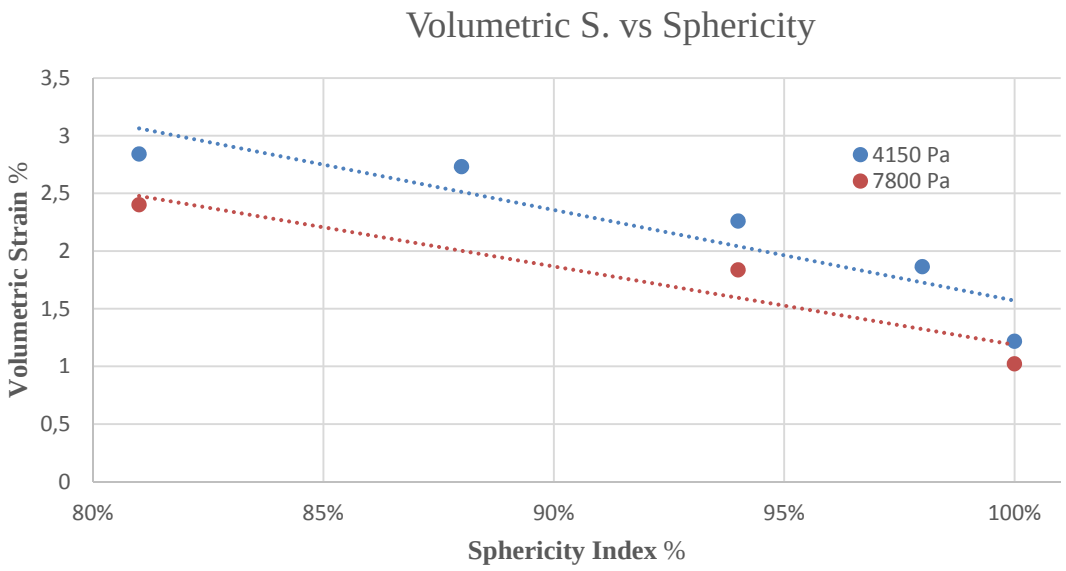

Fig. 7 *Volumetric strain for def. sphericity values at normal stress of 4150 and 7800 Pa*

3.3 AVERAGE CONTACT NUMBERS

The coordination number (CN) is the average of the number of particles in contact with the assembly number of particles. Because the interaction between particles relates to the points of contact, CN is an appropriate parameter to describe the behavior of granular materials.

CN continuously increases as SPH decreases. A decrease in SPH increased the interlocking and CN of the particles. Figure 8 displays that CN rises as SPH, in terms of the sphericity index,

decreases which is inconsistent with the study carried out by [50], who concluded that the number of contacts increased as the eccentricity of the elliptical particles increased, but then decreased with higher values of eccentricity.

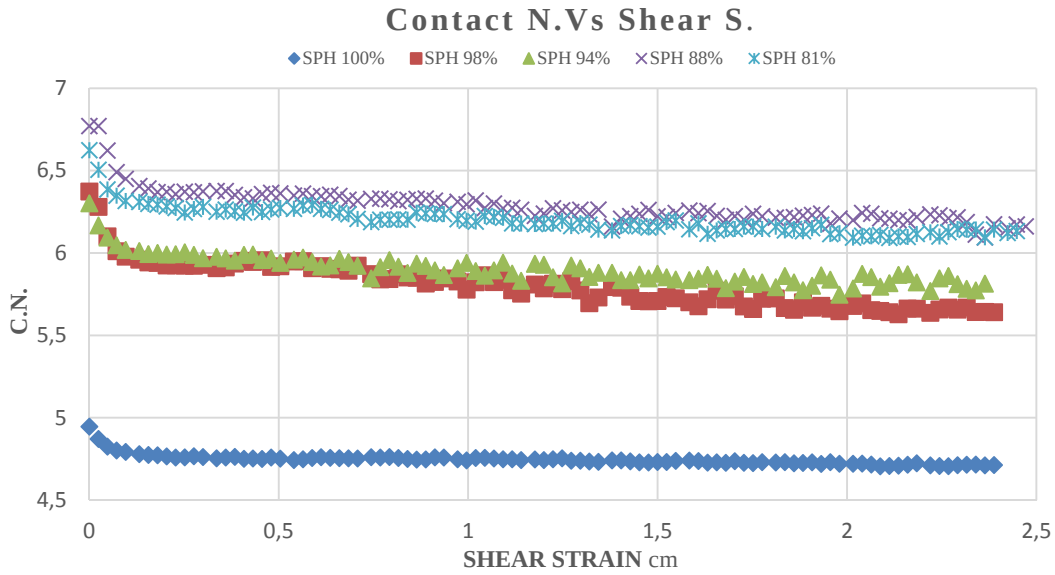

Fig. 8 *Variation of CN versus shear strain for normal stress of 4150 Pa (SPH effect)*

Figure 9 shows that a larger CN was produced, independently of the spherical index, when the sample was subject to high pressure. However, the initial stress causes an immediate decrease in the CN at lower normal stress due to further dilation.

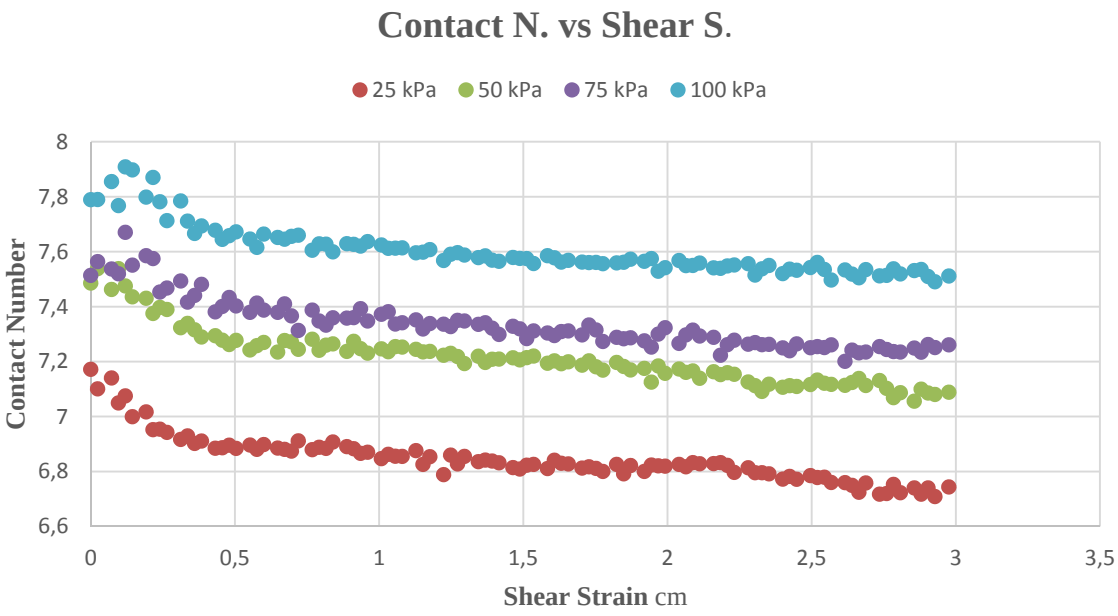

Fig. 9 *Variation of CN versus shear strain for various normal stresses (1.9 mm test)*

3.4 CONTACT FORCE CHAIN

Figures 10 and 11 show the distributions of the inter-particle and particle–wall forces, respectively, for different sphericity values under constant normal stress at various stages of the direct shear test. The particle colors in Figures 10 and 11 are proportional to the intensity of the contact forces. Red, green, and blue particles represent respectively high, moderate, and low forces in the assembly. Before shear loading (at a strain of *0%*). Regardless of particle shape, the interaction forces are uniformly separated in the shear container. As shear force is applied, variations in contact force chains are significantly different at a strain of *15 %* to a strain of *0 %* during shearing. The first stage (Figure 10) shows a thicker contact chain compared to the shearing stage (Figure 11). It is due to the particle dilation behavior during shear that causes the number of contacts to decrease. At the shearing stages, the number of contacts oriented in directions with higher loads increases (i.e. shear direction) and the decrease in shear forces due to contact area reductions. It can also be found, that in the shear stage, the shear force increases in samples with lower sphericity. Assemblies with lower sphericity values displayed a greater increase in strength due to improved interlocking, with both increases in contact numbers and their magnitude in the shear direction. The lower-sphericity samples exhibited a concentration of force near the upper shear cylinder vertical walls. These results are similar to the findings of [51] who reported that strong force chains formed a larger portion of the assembly contacts in the higher granular samples. This rearrangement allows the shear band to shape entirely from the top right to the bottom left of the shear cylinder and provides good transmission of load in the samples. As a consequence, the structure from which force chains are formed is a more stable one. On the other side, the particles positioned apart from the shear band are not involved in the load carrying.

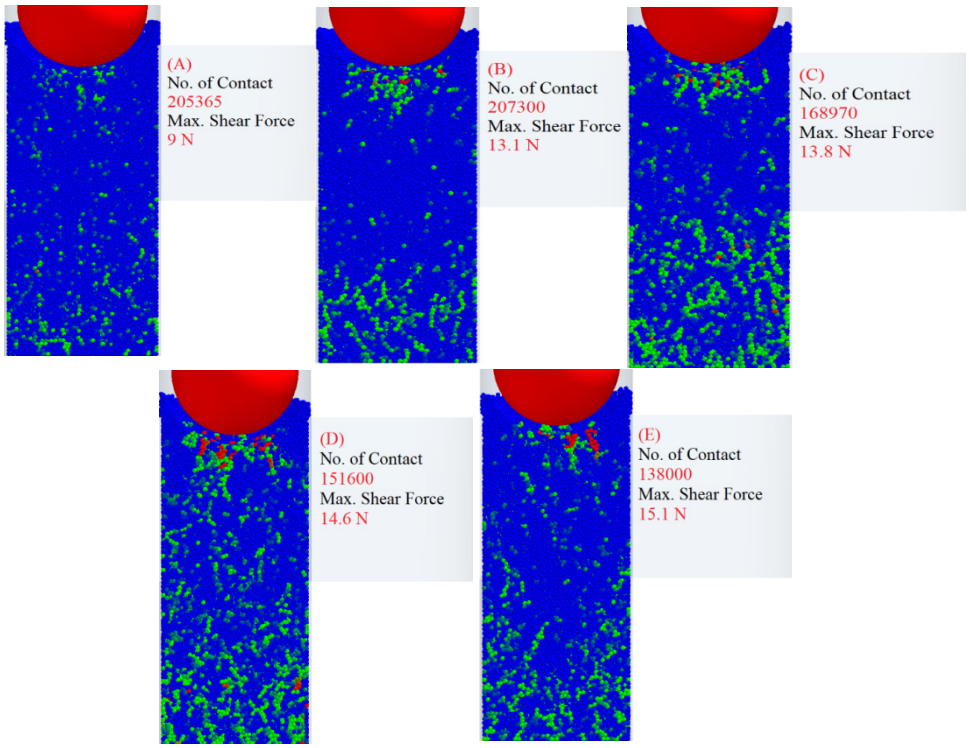

Fig. 10 *Contact force chain distribution for different particle sphericity at shear strain of 0% (Particles SPH = 100%, 98%, 94%, 88%, 81% respectively)*

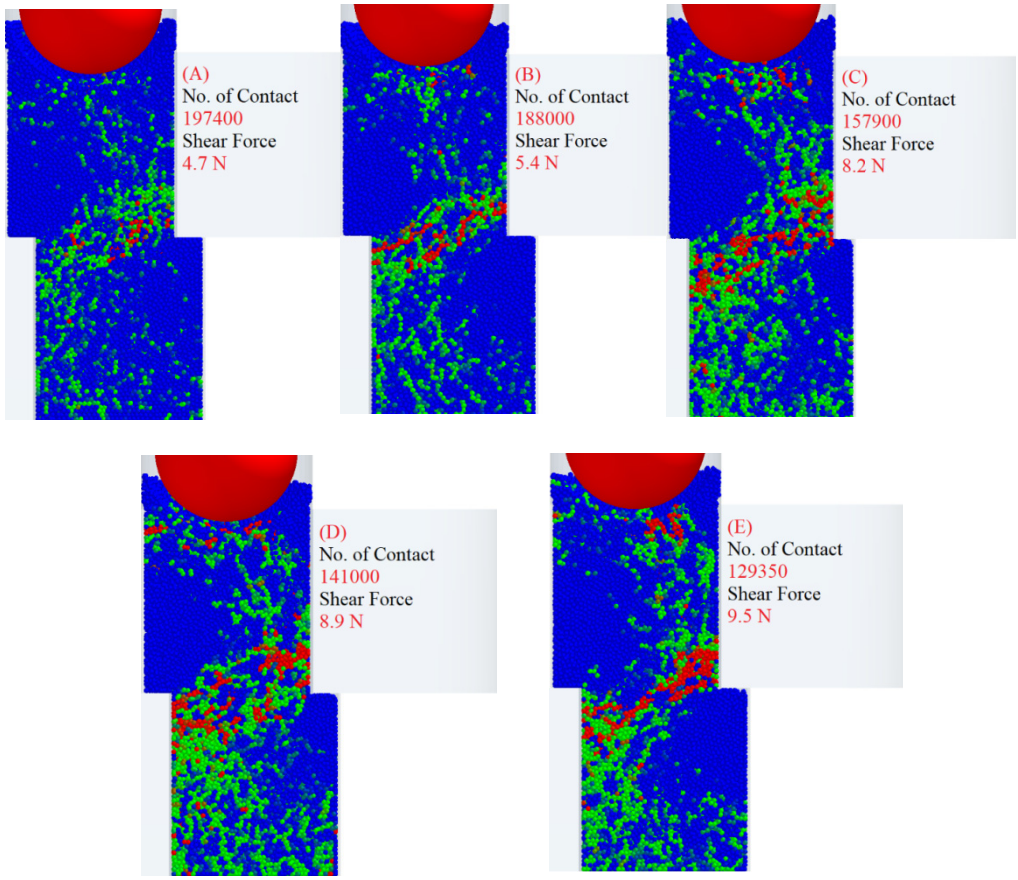

Fig. 11 *Contact force chain distribution for different particle sphericity at shear strain of 15% (Particles SPH = 100%, 98%, 94%, 88%, 81% respectively)*

3.5 SHEAR ZONE AND PARTICLE ROTATION

Particle rotation is a simple method used to evaluate the creation of shear bands in the granular assembly while loading, [52] and [53]. Although the shear band can be evaluated in a direct shear test, there is a need to further analyse the impacts of the non-rounded particles compared to the rounded particles when it comes to the positions and thickness of the shear band. This has been considered in this paper, therefore, (Figure 12) is plotted. This figure shows the accumulated rotation of the particle in the sample at a strain of *15%* under normal stress of *4150 Pa* for sphericity index in which the colors are proportional to their rotations. The particles with higher average rotation values are shown in red color, moderate in green, and low in blue. As shown in Figure 12, the localization of particles with higher rotations for both rounded and non-rounded particles is observed. Particularly for non-rounded particles, the average accumulation rotation is lower than for rounded particles. This occurred more frequently in particles with an SPH of *81%*, as shown in Figures 12 and 13. It is noted that as the interlocking of these particles increases, the average rotation of the particle decreases. For example, by changing the particle shape from spherical SPH *100%* to elongated SPH *81%*, the overall average particle rotation decreases by *40%*. Additionally, Figure 13 shows that the rotation of rounded particles is distributed more uniformly. Particles with an *81 %* SPH display higher rotation near the assembly's core (shear band). It can be noted that the increase in shear strength is followed by a decrease in the rotation zone width and average rotation of the particle [54].

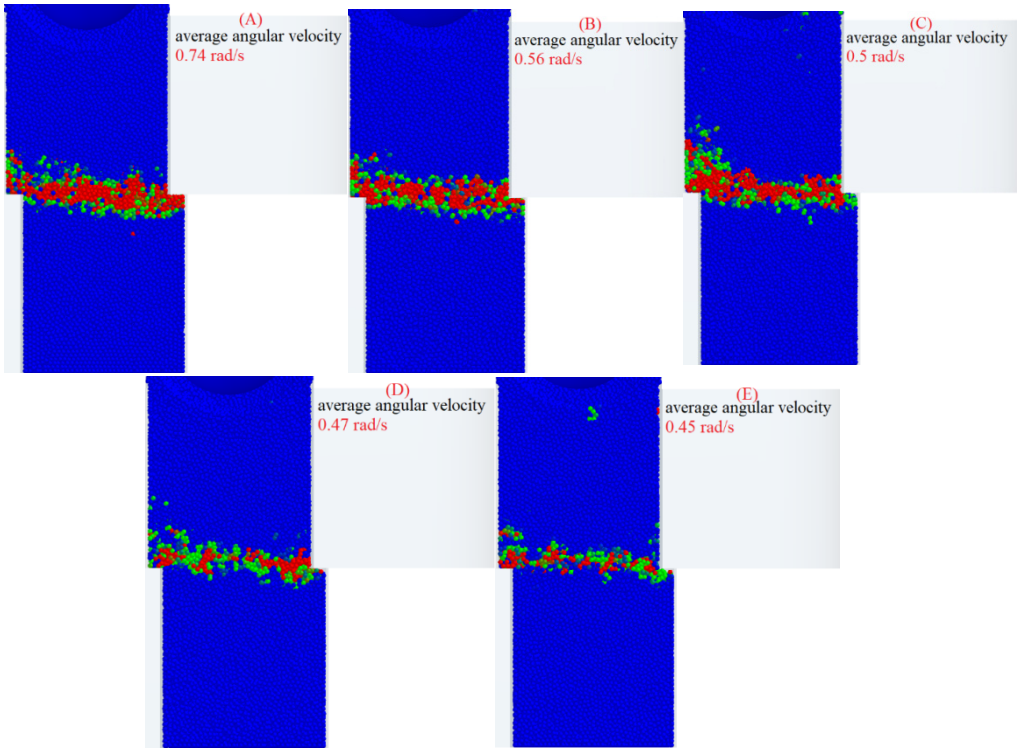

Fig. 12 *Particle rotation at shear strain of 15% for SPH= 100%, 98%, 94%, 88%, 81% respectively*

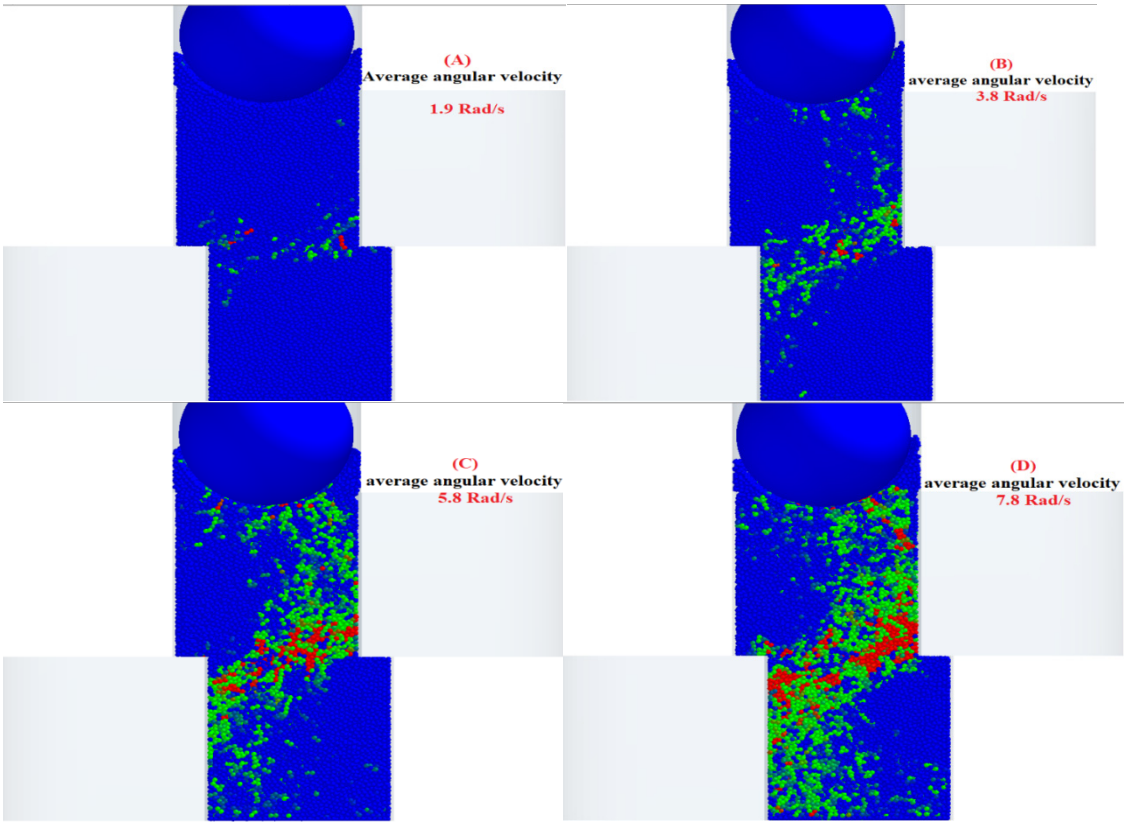

Fig. 13 *Particle rotation at shear strain of 15% for test of 1.9mm at different normal stress = 25 kPa, 50 kPa, 75 kPa, 100 kPa respectively*

As shown in Figure 13, the movement behavior of the particles can be explained as a layer's movement on top of each other. It can be concluded that rotation interaction depends on two features. Firstly, there is the interlocking between the particles, as shown in Figures 11 and 12. Secondly, since the normal force increases the friction between the particles, there will be an increase in rotation interaction because of better contact. It can be noticed that the pattern of rotation follows the distribution of forces in the particle, as rearrangement causes the shear band to form entirely from the upper right to the lower left of the shear cylinder that ensures superior load transfer in the samples.

4. CONCLUSION

The effect of the particle shape properties on particle layer behavior was numerically investigated in this study. The direct shear cylinder test was simulated using a 3D DEM program to produce the actual shape of the particles. Five assemblies were prepared and subjected to different normal stresses with various spherical indexes. The considered particle shape indexes are within the appropriate range.

Both macro-and micro-mechanical responses have been examined, with the main results as follows:

1. In all samples, the dilation decreases as normal stress increases, regardless of the particle shape.
2. Dilation increases by increasing the SPH (sphericity index), but as normal stress increases, the impact of this increase diminishes.
3. Initially, shear strength decreases and dilation increases with an increase in spherical values. The highest increase in strength occurs at *81%* SPH.
4. The effects of shape index on the variance of the coordination number (CN) are consistent with the dilation behavior of the assemblies. Increased dilation is accompanied by a decrease in CN.
5. The movement behavior of the particles can be explained as a movement of layers on top of each other.
6. In the initial stage of shearing, the inter-particle force are distributed equally in all assemblies, and then the number of contacts oriented in directions with higher stress and their magnitude increases.
7. For rounded shape particles, the average particle rotation is greater than for non-rounded shape particles. Despite the decrease in the sample's average particle rotation with an SPH of *81%*, the number of particles with higher rotation increases near the shear surface due to better interlocking of particles. In addition, the width of the shear zone in these samples is smaller than for the rounded particles.

In general, sphericity variation has a significant individual effect on ballast sample shear strength.

5. ACKNOWLEDGMENT

This work was supported by the Stipendium Hungaricum Program and by the Mechanical Engineering Doctoral School, Szent István University, Gödöllő, Hungary.

6. REFERENCES

[1] A.S.J. Suiker, E.T. Selig, R. Frenkel, Static and cyclic triaxial testing of ballast and subballast, *J. Geotech. Geoenvironmental Eng.*, Vol. 131, No. 6, pp. 771–782, Jun. 2005. https://doi.org/10.1061/(ASCE)1090-0241(2005)131:6(771)

[2] A.M. Remennikov, S. Kaewunruen, A review of loading conditions for railway track structures due to train and track vertical interaction, *Structural Control and Health Monitoring*, Vol. 15, No. 2, pp. 207–234, Mar. 2008. https://doi.org/10.1002/stc.227

[3] J. Lackenby, B. Indraratna, G. McDowell, D. Christie, Effect of confining pressure on ballast degradation and deformation under cyclic triaxial loading, *Géotechnique*, Vol. 57, No. 6, pp. 527–536, Aug. 2007. https://doi.org/10.1680/geot.2007.57.6.527

[4] G.P. Raymond, J.R. Davies, Triaxial tests on dolomite railroad ballast, *ASCE J. Geotech. Eng. Div.*, Vol. 104, No. 6, pp. 737–751, 1978. https://doi.org/10.1016/0148-9062(78)91498-5

[5] B. Indraratna, H. Khabbaz, W. Salim, D. Christie, Geotechnical properties of ballast and the role of geosynthetics in rail track stabilisation, *Proc. Inst. Civ. Eng. - Gr. Improv.*, Vol. 10, No. 3, pp. 91–101, Jul. 2006. https://doi.org/10.1680/grim.2006.10.3.91

[6] C.N. Cunningham, T.M. Evans, A.A. Tayebali, Gradation effects on the mechanical response of crushed stone aggregate, *Int. J. Pavement Eng.*, Vol. 14, No. 3, pp. 231–241, Apr. 2013. https://doi.org/10.1080/10298436.2012.690518

[7] B. Indraratna, Y. Sun, S. Nimbalkar, Laboratory Assessment of the Role of Particle Size Distribution on the Deformation and Degradation of Ballast under Cyclic Loading, *J. Geotech. Geoenvironmental Eng.*, Vol. 142, No. 7, p. 04016016, Jul. 2016. https://doi.org/10.1061/(ASCE)GT.1943-5606.0001463

[8] H. Huang, E. Tutumluer, W. Dombrow, Laboratory Characterization of Fouled Railroad Ballast Behavior, *Transp. Res. Rec. J. Transp. Res. Board*, Vol. 2117, No. 1, pp. 93–101, Jan. 2009. https://doi.org/10.3141/2117-12

[9] H. Huang, E. Tutumluer, Image-Aided Element Shape Generation Method in Discrete-Element Modeling for Railroad Ballast, *J. Mater. Civ. Eng.*, Vol. 26, No. 3, pp. 527–535, Mar. 2014. https://doi.org/10.1061/(ASCE)MT.1943-5533.0000839

[10] V.N. Trinh et al., Mechanical characterisation of the fouled ballast in ancient railway track substructure by large-scale triaxial tests, *Soils Found.*, Vol. 52, No. 3, pp. 511–523, Jun. 2012. https://doi.org/10.1016/j.sandf.2012.05.009

[11] Y. Qian, D. Mishra, E. Tutumluer, H.A. Kazmee, Characterization of geogrid reinforced ballast behavior at different levels of degradation through triaxial shear strength test and discrete element modeling, *Geotext. Geomembranes*, Vol. 43, No. 5, pp. 393–402, Oct. 2015. https://doi.org/10.1016/j.geotexmem.2015.04.012

[12] W.L. Lim, G.R. Mcdowell, A.C. Collop, The application of Weibull statistics to the strength of railway ballast, *Granul. Matter*, Vol. 6, pp. 229–237, 2004. https://doi.org/10.1007/s10035-004-0180-z

[13] A. Sevi, L. Ge, Cyclic behaviors of railroad ballast within the parallel gradation scaling framework, *J. Mater. Civ. Eng.*, Vol. 24, No. 7, pp. 797–804, Jul. 2012.

https://doi.org/10.1061/(ASCE)MT.1943-5533.0000460

[14] E. Tutumluer, H. Huang, Y. Hashash, Aggregate Shape Effects on Ballast Tamping and Railroad Track Lateral Stability, Sep. 2006. Accessed: Jul. 22, 2020. [Online]. Available: https://www.researchgate.net/publication/237116793

[15] J.P. Latham, A. Munjiza, X. Garcia, J. Xiang, R. Guises, Three-dimensional particle shape acquisition and use of shape library for DEM and FEM/DEM simulation, *Miner. Eng.*, Vol. 21, No. 11, pp. 797–805, Oct. 2008.

https://doi.org/10.1016/j.mineng.2008.05.015

[16] R. Guises, J. Xiang, J.P. Latham, A. Munjiza, Granular packing: Numerical simulation and the characterisation of the effect of particle shape, *Granul. Matter*, Vol. 11, No. 5, pp. 281–292, Oct. 2009. https://doi.org/10.1007/s10035-009-0148-0

[17] M. Koohmishi, M. Palassi, Evaluation of the Strength of Railway Ballast Using Point Load Test for Various Size Fractions and Particle Shapes, *Rock Mech. Rock Eng.*, Vol. 49, No. 7, pp. 2655–2664, Jul. 2016. https://doi.org/10.1007/s00603-016-0914-3

[18] D. Li, J. Hyslip, T. Sussmann, S. Chrismer, *Railway Geotechnics*, 1st edition, CRC Press, London 2015. https://doi.org/10.1201/b18982

[19] Y. Guo, V. Markine, J. Song, G. Jing, Ballast degradation: Effect of particle size and shape using Los Angeles Abrasion test and image analysis, *Constr. Build. Mater.*, Vol. 169, pp. 414–424, Apr. 2018. https://doi.org/10.1016/j.conbuildmat.2018.02.170

[20] S. Lobo-Guerrero, L.E. Vallejo, Discrete element method analysis of railtrack ballast degradation during cyclic loading, *Granul. Matter*, Vol. 8, No. 3-4, pp. 195–204, 2006.

https://doi.org/10.1007/s10035-006-0006-2

[21] S. Abedi, A.A. Mirghasemi, Particle shape consideration in numerical simulation of assemblies of irregularly shaped particles, *Particuology*, Vol. 9, No. 4, pp. 387–397, Aug. 2011. https://doi.org/10.1016/j.partic.2010.11.005

[22] P.A. Cundall, O.D.L. Strack, A discrete numerical model for granular assemblies, *Géotechnique*, Vol. 29, No. 1, pp. 47–65, Mar. 1979.

https://doi.org/10.1680/geot.1979.29.1.47

[23] L. Rothenburg, R.J. Bathurst, Micromechanical features of granular assemblies with planar eliptical particles, *Géotechnique*, Vol. 42, No. 1, pp. 79–95, Mar. 1992. https://doi.org/10.1680/geot.1992.42.1.79

[24] A.A. Mirghasemi, L. Rothenburg, E.L. Matyas, Numerical simulations of assemblies of two-dimensional polygon-shaped particles and effects of confining pressure on shear strength, *Soils Found.*, Vol. 37, No. 3, pp. 43–52, Sep. 1997.

https://doi.org/10.3208/sandf.37.3_43

[25] A.V. Potapov, C.S. Campbell, A fast model for the simulation of non-round particles, *Granul. Matter*, Vol. 1, No. 1, pp. 9–14, 1998. https://doi.org/10.1007/PL00010910

[26] R.P. Jensen, P.J. Bosscher, M.E. Plesha, T.B. Edil, DEM simulation of granular media-structure interface: effects of surface roughness and particle shape, *Int. J. Numer. Anal. Methods Geomech.*, Vol. 23, No. 6, pp. 531–547, May 1999.

https://doi.org/10.1002/(SICI)1096-9853(199905)23:6<531::AID-NAG980>3.0.CO;2-V

[27] J.F. Favier, M.H. Abbaspour-Fard, M. Kremmer, Modeling Nonspherical Particles Using Multisphere Discrete Elements, *J. Eng. Mech.*, Vol. 127, No. 10, pp. 971–977, Oct. 2001. https://doi.org/10.1061/(ASCE)0733-9399(2001)127:10(971)

[28] E. Tutumluer, Y. Qian, Y.M.A. Hashash, J. Ghaboussi, D.D. Davis, Discrete element modelling of ballasted track deformation behaviour, *Int. J. Rail Transp.*, Vol. 1, No. 1–2, pp. 57–73, Feb. 2013. https://doi.org/10.1080/23248378.2013.788361

[29] X. Bian, H. Huang, E. Tutumluer, Y. Gao, Critical particle size' and ballast gradation studied by Discrete Element Modeling, *Transp. Geotech.*, Vol. 6, pp. 38–44, Mar. 2016.

https://doi.org/10.1016/j.trgeo.2016.01.002

[30] G. Saussine et al., Modelling ballast behaviour under dynamic loading. Part 1: A 2D polygonal discrete element method approach, *Comput. Methods Appl. Mech. Eng.*, Vol. 195, No. 19-22, pp. 2841–2859, 2006. https://doi.org/10.1016/j.cma.2005.07.006

[31] Y. Qian, S.J. Lee, E. Tutumluer, Y.M.A. Hashash, D. Mishra, J. Ghaboussi, Simulating Ballast Shear Strength from Large-Scale Triaxial Tests, *Transp. Res. Rec. J. Transp. Res. Board*, Vol. 2374, No. 1, pp. 126–135, Jan. 2013. https://doi.org/10.3141/2374-15

[32] J. Eliáš, Simulation of railway ballast using crushable polyhedral particles, *Powder Technol.*, Vol. 264, pp. 458–465, Sep. 2014.

https://doi.org/10.1016/j.powtec.2014.05.052

[33] S. Ji, S. Sun, Y. Yan, Discrete element modeling of dynamic behaviors of railway ballast under cyclic loading with dilated polyhedra, *Int. J. Numer. Anal. Methods Geomech.*, Vol. 41, No. 2, pp. 180–197, Feb. 2017. https://doi.org/10.1002/nag.2549

[34] B. Indraratna, P.K. Thakur, J.S. Vinod, Experimental and Numerical Study of Railway Ballast Behavior under Cyclic Loading, *Int. J. Geomech.*, Vol. 10, No. 4, pp. 136–144, Aug. 2010. https://doi.org/10.1061/(ASCE)GM.1943-5622.0000055

[35] G. Jing, K. Feng, L. Gao, J. Wang, DEM simulation of ballast degradation and breakage under cyclic loading, *Xinan Jiaotong Daxue Xuebao/Journal Southwest Jiaotong Univ.*, Vol. 47, No. 2, pp. 187–191, 2012.

http://journal16.magtechjournal.com/Jweb_xnjd/EN/10.3969/j.issn.0258-2724.2012.02.003

[36] T. Matsushima, H. Saomoto, Discrete element modeling for irregularly Y-shaped sand grains, *Proc. NUMGE2002 Numer. Methods Geotech. Eng.*, pp. 239–246, 2002, Accessed: Jul. 22, 2020. [Online]. Available:

https://pascal-francis.inist.fr/vibad/index.php?action=getRecordDetail&idt=16398173

[37] C. Chen, G.R. McDowell, N.H. Thom, Discrete element modelling of cyclic loads of geogrid-reinforced ballast under confined and unconfined conditions, *Geotext. Geomembranes*, Vol. 35, pp. 76–86, Dec. 2012.

https://doi.org/10.1016/j.geotexmem.2012.07.004

[38] B. Indraratna, N.T. Ngo, C. Rujikiatkamjorn, J.S. Vinod, Behavior of fresh and fouled railway ballast subjected to direct shear testing: Discrete element simulation, *Int. J. Geomech.*, Vol. 14, No. 1, pp. 34–44, Feb. 2014.

https://doi.org/10.1061/(ASCE)GM.1943-5622.0000264

[39] N.T. Ngo, B. Indraratna, C. Rujikiatkamjorn, DEM simulation of the behaviour of geogrid stabilised ballast fouled with coal, *Comput. Geotech.*, Vol. 55, pp. 224–231, Jan. 2014. https://doi.org/10.1016/j.compgeo.2013.09.008

[40] H. Xu, S.J. Liao, Laminar flow and heat transfer in the boundary-layer of non-Newtonian fluids over a stretching flat sheet, *Comput. Math. with Appl.*, Vol. 57, No. 9, pp. 1425–1431, 2009. https://doi.org/10.1016/j.camwa.2009.01.029

[41] A. Danesh, M. Palassi, A.A. Mirghasemi, Evaluating the influence of ballast degradation on its shear behaviour, *Int. J. Rail Transp.*, Vol. 6, No. 3, pp. 145–162, Jul. 2018. https://doi.org/10.1080/23248378.2017.1411212

[42] P.A. Cundall, O.D.L. Strack, "Cundall_Strack.Pdf." pp. 47–65, 1979.

https://doi.org/10.1680/geot.1979.29.1.47

[43] I. Oldal, F. Safranyik, Extension of silo discharge model based on discrete element method, *J. Mech. Sci. Technol.*, Vol. 29, No. 9, pp. 3789–3796, 2015.

https://doi.org/10.1007/s12206-015-0825-3

[44] I. Keppler, L. Kocsis, I. Oldal, I. Farkas, A. Csatar, Grain velocity distribution in a mixed flow dryer, *Adv. Powder Technol.*, Vol. 23, No. 6, pp. 824–832, 2012. https://doi.org/10.1016/j.apt.2011.11.003

[45] C. González-Montellano, A. Ramírez, J.M. Fuentes, F. Ayuga, Numerical effects derived from en masse filling of agricultural silos in DEM simulations, *Comput. Electron. Agric.*, Vol. 81, pp. 113–123, 2012. https://doi.org/10.1016/j.compag.2011.11.013

[46] V. Kostkanová, I. Herle, Measurement of wall friction in direct shear tests on soft soil, *Acta Geotech.*, Vol. 7, No. 4, pp. 333–342, Dec. 2012.

https://doi.org/10.1007/s11440-012-0167-6

[47] W.C. Krumbein, Measurement and Geological Significance of Shape and Roundness of Sedimentary Particles, *SEPM J. Sediment. Res.*, Vol. 11, No. 2, pp. 64–72, Aug. 1941. https://doi.org/10.1306/D42690F3-2B26-11D7-8648000102C1865D

[48] J. Gong, J. Liu, Effect of aspect ratio on triaxial compression of multi-sphere ellipsoid assemblies simulated using a discrete element method, *Particuology*, Vol. 32, pp. 49–62, Jun. 2017. https://doi.org/10.1016/j.partic.2016.07.007

[49] L. Rothenburg, R.J. Bathurst, Numerical simulation of idealized granular assemblies with plane elliptical particles, *Comput. Geotech.*, Vol. 11, No. 4, pp. 315–329, Jan. 1991.

https://doi.org/10.1016/0266-352X(91)90015-8

[50] R. Asadi, A.A. Mirghasemi, Numerical investigation of particle shape on mechanical behaviour of unsaturated granular soils using elliptical particles, *Adv. Powder Technol.*, Vol. 29, No. 12, pp. 3087–3099, Dec. 2018. https://doi.org/10.1016/j.apt.2018.08.018

[51] Y. Yang, J.F. Wang, Y.M. Cheng, Quantified evaluation of particle shape effects from micro-to-macro scales for non-convex grains, *Particuology*, Vol. 25, pp. 23–35, Apr. 2016. https://doi.org/10.1016/j.partic.2015.01.008

[52] M. Oda, H. Kazama, Microstructure of shear bands and its relation to the mechanisms of dilatancy and failure of dense granular soils, Géotechnique, Vol. 48, No. 4, pp. 465–481, Aug. 1998. https://doi.org/10.1680/geot.1998.48.4.465

[53] Z. Mahmood, K. Iwashita, A simulation study of microstructure evolution inside the shear band in biaxial compression test, *Int. J. Numer. Anal. Methods Geomech.*, Vol. 35, No. 6, pp. 652–667, Apr. 2011. https://doi.org/10.1002/nag.917

[54] A. Danesh, A.A. Mirghasemi, M. Palassi, Evaluation of particle shape on direct shear mechanical behavior of ballast assembly using discrete element method (DEM), *Transp. Geotech.*, Vol. 23, p. 100357, Jun. 2020. https://doi.org/10.1016/j.trgeo.2020.100357